Acta Mechanica Solida Sinica, Vol. 35, No. 4, August, 2022, 694–704 ISSN 1860-2134
https://doi.org/10.1007/s10338-022-00310-x

Guided Wave Propagation in Multilayered Two-dimensional Quasicrystal Plates with Imperfect Interfaces

Xin Feng[1,2] **Liangliang Zhang**[1] **Zhiming Hu**[1] **Han Zhang**[3⋆] **Yang Gao**[1⋆]
([1] *College of Science, China Agricultural University, Beijing 100083, China*)
([2] *College of Engineering, China Agricultural University, Beijing 100083, China*)
([3] *China State Key Laboratory of Acoustics, Institute of Acoustics, Chinese Academy of Sciences, Beijing 100190, China*)

Received 6 October 2021; revision received 11 January 2022; Accepted 12 January 2022; published online 17 February 2022

ABSTRACT An analytical solution of the guided wave propagation in a multilayered two-dimensional decagonal quasicrystal plate with imperfect interfaces is derived. According to the elastodynamic equations of quasicrystals (QCs), the wave propagating problem in the plate is converted into a linear control system by employing the state-vector approach, from which the general solutions of the extended displacements and stresses can be obtained. These solutions along the thickness direction are utilized to derive the propagator matrix which connects the physical variables on the lower and upper interfaces of each layer. The special spring model, which describes the discontinuity of the physical quantities across the interface, is introduced into the propagator relationship of the multilayered structure. The total propagator matrix can be used to propagate the solutions in each interface and each layer about the multilayered plate. In addition, the traction-free boundary condition on the top and bottom surfaces of the laminate is considered to obtain the dispersion equation of wave propagation. Finally, typical numerical examples are presented to illustrate the marked influences of stacking sequence and interface coefficients on the dispersion curves and displacement mode shapes of the QC laminates.

KEY WORDS Two-dimensional QC materials, Wave propagation, Dispersion curve, State vector approach, Propagator matrix, Imperfect interface

1. Introduction

As a novel kind of solid material, QCs have long-range order with symmetries that are prohibitive in conventional crystals [1, 2], such as fivefold, eightfold, tenfold, and twelvefold rotational symmetries. The ordered but quasi-periodic atom arrangement in QCs makes them possess a variety of excellent properties, such as high hardness, high toughness, high abrasion resistance, high resistivity, low friction coefficient, low thermal conductivity, and so on [2–4]. Due to these complex physical properties, QCs have some potential applications, including thin films [5], coatings [6], and structural enhancement phase [7] in composites. The multilayered plate model provides significant instructions for understanding the characteristics of QC coatings or thin films.

⋆ Corresponding authors. E-mails:zhanghan@mail.ioa.ac.cn; gaoyangg@gmail.com

To predict the mechanical properties of the QC multilayered structure, various analytical/numerical studies and mechanical models of these multiphase and multifunctional materials have been carried out, which include research on the static response [8], free vibration [9], and the effective bulk material properties [10, 11]. Based on linear elastic theory, Yang et al. [12] obtained the exact solution of the 2D decagonal QC laminate with different quasi-periodic directions. By using the pseudo-Stroh formalism, Guo et al. [13] developed a thermoelastic solution of the 2D QC plane with a conductive elliptic hole. Li et al. [14] investigated the dynamic behaviors of 2D QC nanoplates with nonlocal effect, and analyzed the effect of non-local parameters on the natural frequencies and mode shapes of simply-supported laminates. Huang et al. [15] derived the dynamic response of 2D piezoelectric QC cylindrical shells by employing the state-space method. To the best of the authors' knowledge, however, little literature [16, 17] has investigated wave propagation in QC laminates. In industry practice, nondestructive inspection based on the propagation of elastic waves that relies generally on the calculation of dispersion curves plays an important role in damage identification in multilayered structures [18–20]. From this perspective, the derivation of the dispersion relation is one of the significant essentials for the inspection of 2D QC multilayered structures.

The interfacial imperfections, including the homogeneous and inhomogeneous weak interfaces, describe a significant factor in the failure of laminated composite materials, which may cause the delamination and cracking problems for the multilayered composite structures. These disadvantages limit the application of laminates [21]. For multilayered structures with inhomogeneous interfaces, researchers have made some progress in the studies [22–25]. In addition, several numerical methods, including the finite element methods [26, 27], boundary element methods [28], Muller's method [29], and the first-order plate theory [30], can be used to derive the solutions of static analysis and dynamic response for plates with homogeneous weak interfaces. Furthermore, the spring layer model [31] has been proved to be powerful for studying multilayered structures with weak imperfections. Compared with other methods, this model can be perfectly combined with the propagator matrix to obtain an exact solution. By using the extended Stroh formalism and the spring model, Vattré et al. [32, 33] obtained the exact solutions of fully coupled thermoelastic laminates with imperfect interfaces. Chen et al. [34] discussed the static and free vibration of simply-supported cross-ply laminates featuring interlaminar bonding imperfections. This model has been proved to be a useful tool to study the properties of structures with imperfect interfaces. However, few pieces of literature [35, 36] have investigated the static response and free vibration of the multilayered QC structures with a weak interface. And to the best of the authors' knowledge, the wave propagation in 2D QC laminates with an imperfect interface has not yet been reported.

In this paper, based on the QC elastodynamics theory given by Bak [37, 38], the wave propagation characteristics in 2D QC laminates with bonding imperfections are derived by using the state vector approach and the propagator matrix method. The generalized spring model is applied to simulate the discontinuity of variables between layers to derive the global propagator matrix, and the dispersion curves and mode shapes are obtained. Numerical examples are also presented to show the features of the dispersion curves and the corresponding modal shapes, which can be applied to guide the nondestructive testing and evaluations of multilayer QC wave devices.

2. Theoretical Formulation

Consider an N-layer 2D decagonal QC plate with an imperfect interface. The atomic arrangement of the 2D decagonal QC is quasi-periodic in the x-y infinite plane and periodic along the z-direction. The relationship between the global Cartesian coordinate system and the local material coordinate system of the plate is assumed to be $(x, y, z) = (x_1, x_2, x_3)$. The thickness $h_p = z_p - z_{p-1}$ $(p = 1, 2, 3, \ldots, N)$ is defined as the p-th layer in the multilayer plate, and its upper and lower interfaces are bounded by z_p and z_{p-1}, respectively. Meanwhile, the bottom and top surfaces of the laminate are $z_0 = 0$ and $z_N = H$, respectively.

2.1. Governing Equations

In this part, the material local coordinate system (x_1, x_2, x_3) is utilized to describe the basic equations of 2D decagonal QC materials. According to the linear elastic theory of QCs [2], the generalized relationship of strain-displacement for 2D QCs is

$$\varepsilon_{ij} = (u_{i,j} + u_{j,i})/2,\ W_{kj} = w_{k,j} \tag{1}$$

where $i,\ j = 1,\ 2,\ 3$, and $k = 1,\ 2$. ε_{ij} and W_{kj} are the strains in the phonon and phason fields, respectively. u_i and w_k denote the phonon and phason displacements, respectively. The subscript comma is defined as partial differentiation with respect to the axis.

Employing Bak's theory [37, 38] as the QC elastodynamics model for wave propagation, the equations of motion in the absence of body forces are

$$\sigma_{ij,j} = \rho_1 \frac{\partial^2 u_i}{\partial t^2},\ H_{kj,j} = \rho_2 \frac{\partial^2 w_k}{\partial t^2} \tag{2}$$

where ρ_1 and ρ_2 are the phonon and phason mass densities, respectively; t is time; σ_{ij} and H_{kj} denote the phonon and phason stresses, respectively.

The stress–strain relationship for 2D decagonal QCs with point groups $10mm$, 1022, $\bar{1}\bar{0}m2$, and $10/mmm$ [13] can be expressed as

$$\begin{aligned}
&\sigma_{11} = C_{11}\varepsilon_{11} + C_{12}\varepsilon_{22} + C_{13}\varepsilon_{33} + R_1 (W_{11} + W_{22})\\
&\sigma_{22} = C_{12}\varepsilon_{11} + C_{11}\varepsilon_{22} + C_{13}\varepsilon_{33} - R_1 (W_{11} + W_{22})\\
&\sigma_{33} = C_{13}\varepsilon_{11} + C_{13}\varepsilon_{22} + C_{33}\varepsilon_{33}\\
&\sigma_{23} = \sigma_{32} = 2C_{44}\varepsilon_{23}\\
&\sigma_{31} = \sigma_{13} = 2C_{44}\varepsilon_{13}\\
&\sigma_{12} = \sigma_{21} = 2C_{66}\varepsilon_{12} - R_1 W_{12} + R_1 W_{21}\\
&H_{11} = R_1 (\varepsilon_{11} - \varepsilon_{22}) + K_1 W_{11} + K_2 W_{22}\\
&H_{22} = R_1 (\varepsilon_{11} - \varepsilon_{22}) + K_1 W_{22} + K_2 W_{11}\\
&H_{23} = K_4 W_{23}\\
&H_{12} = -2R_1\varepsilon_{12} + K_1 W_{12} - K_2 W_{21}\\
&H_{13} = K_4 W_{13}\\
&H_{21} = 2R_1\varepsilon_{12} - K_2 W_{12} + K_1 W_{21}
\end{aligned} \tag{3}$$

where C_{11}, C_{12}, C_{13}, C_{33}, and C_{44} are the elastic constants with the relationship $2C_{66} = C_{11} - C_{12}$ in the phonon field, K_1, K_2, K_4, and R_1 represent the phason elastic constants and the phonon-phason coupling elastic constant, respectively.

2.2. State Vector Formulations

The Cartesian coordinate system $(x,\ y,\ z)$ is utilized to describe the guided wave propagation in 2D QC laminates. Substituting Eqs. (1) and (3) into Eq. (2), and according to the state vector approach for QC plate, the state equations can be written as

$$\frac{\partial}{\partial z}\boldsymbol{\theta} = \boldsymbol{A\theta} \tag{4}$$

where $\boldsymbol{\theta} = \{u_x, u_y,\ w_x, w_y, \sigma_{zz}, \sigma_{xz}, \sigma_{yz}, H_{xz}, H_{yz}, u_z\}^{\mathrm{T}}$ is the state variables, in which the superscript 'T' denotes transpose; and the state transition matrix $\boldsymbol{A}$ is

$$\boldsymbol{A} = \begin{bmatrix} \mathbf{0} & \boldsymbol{A}_1 \\ \boldsymbol{A}_2 & \mathbf{0} \end{bmatrix} \tag{5}$$

The submatrices $\boldsymbol{A}_1$ and $\boldsymbol{A}_2$ in Eq. (5) are

$$\boldsymbol{A}_1 = \begin{bmatrix} a_5 & & & & \\ 0 & a_5 & & \text{Sym} & \\ 0 & 0 & b_3 & & \\ 0 & 0 & 0 & b_3 & \\ -\frac{\partial}{\partial x} & -\frac{\partial}{\partial y} & 0 & 0 & \rho_1 \frac{\partial^2}{\partial t^2} \end{bmatrix} \tag{6}$$

$$\boldsymbol{A}_2=\begin{bmatrix} -a_1\frac{\partial^2}{\partial x^2}-a_4\frac{\partial^2}{\partial y^2}+\rho_1\frac{\partial^2}{\partial t^2} & & & & \\ -\left(a_2+a_6\right)\frac{\partial^2}{\partial x\partial y} & -a_4\frac{\partial^2}{\partial x^2}-a_1\frac{\partial^2}{\partial y^2}+\rho_1\frac{\partial^2}{\partial t^2} & & & \text{Sym} \\ -b_1\frac{\partial^2}{\partial x^2}+b_1\frac{\partial^2}{\partial y^2} & 2b_1\frac{\partial^2}{\partial x\partial y} & -b_2\Delta+\rho_2\frac{\partial^2}{\partial t^2} & & \\ -2b_1\frac{\partial^2}{\partial x\partial y} & -b_1\frac{\partial^2}{\partial x^2}+b_1\frac{\partial^2}{\partial y^2} & 0 & -b_2\Delta+\rho_2\frac{\partial^2}{\partial t^2} & \\ a_3\frac{\partial}{\partial x} & a_3\frac{\partial}{\partial y} & 0 & 0 & a_6 \end{bmatrix} \tag{7}$$

where “Sym” denotes a symmetric matrix, Δ is the 2D Laplace operator, and the coefficients are written as follows

$$\begin{aligned} &a_1=C_{11}-\tfrac{C_{13}^2}{C_{33}},\ a_2=C_{12}-\tfrac{C_{13}^2}{C_{33}},\ a_3=-\tfrac{C_{13}}{C_{33}},\ a_4=C_{66},\ a_5=\tfrac{1}{C_{44}},\ a_6=\tfrac{1}{C_{33}} \\ &b_1=R_1,\ b_2=K_1,\ b_3=\tfrac{1}{K_4} \end{aligned} \tag{8}$$

2.3. Dispersion Relation

It is assumed that the guided wave motion in the QC plate and its propagating angle α is measured from the positive x-axis in the anti-clockwise direction. Thus, the solutions of Eq. (4) can be written as

$$\boldsymbol{\theta}=\tilde{\boldsymbol{\theta}}\left(z\right)\mathrm{e}^{\mathrm{i}(px+qy-\omega t)} \tag{9}$$

where ω is the angular frequency, and imaginary $\mathrm{i}=\sqrt{-1}$; p and q are the two components of the wave vector which are expressed as

$$p=k\cos\alpha,\ q=k\sin\alpha \tag{10}$$

where k is the magnitude of the wavenumber along the propagation direction.

In order to avoid imaginary number calculation, $\boldsymbol{\theta}(z)$ in Eq. (9) is rewritten as:

$$\tilde{\boldsymbol{\theta}}\left(z\right)=\left\{\tilde{u}_x,\ \tilde{u}_y,\ \tilde{w}_x,\ \tilde{w}_y,\ \mathrm{i}\tilde{\sigma}_{zz},\ \tilde{\sigma}_{xz},\ \tilde{\sigma}_{yz},\ \tilde{H}_{xz},\ \tilde{H}_{yz},\ \mathrm{i}\tilde{u}_z\right\}^{\mathrm{T}} \tag{11}$$

Substituting Eq. (9) into Eq. (4), the state equations can be expressed as

$$\frac{\mathrm{d}}{\mathrm{d}z}\tilde{\boldsymbol{\theta}}\left(z\right)=\tilde{\boldsymbol{A}}\left(\omega,k\right)\tilde{\boldsymbol{\theta}}\left(z\right) \tag{12}$$

where

$$\tilde{\boldsymbol{A}}\left(\omega,k\right)=\begin{bmatrix}\boldsymbol{0} & \tilde{\boldsymbol{A}}_1\left(\omega,k\right)\\ \tilde{\boldsymbol{A}}_2\left(\omega,k\right) & \boldsymbol{0}\end{bmatrix} \tag{13}$$

with

$$\tilde{\boldsymbol{A}}_1\left(\omega,k\right)=\begin{bmatrix} a_5 & 0 & 0 & 0 & -p\\ 0 & a_5 & 0 & 0 & -q\\ 0 & 0 & b_3 & 0 & 0\\ 0 & 0 & 0 & b_3 & 0\\ p & q & 0 & 0 & -\rho_1\omega^2 \end{bmatrix} \tag{14}$$

$$\tilde{\boldsymbol{A}}_2\left(\omega,k\right)=\begin{bmatrix} a_1p^2+a_4q^2-\rho_1\omega^2 & \left(a_2+a_4\right)pq & b_1p^2-b_1q^2 & 2b_1pq & a_3p\\ \left(a_2+a_4\right)pq & a_1q^2+a_4p^2-\rho_1\omega^2 & -2b_1pq & b_1p^2-b_1q^2 & a_3q\\ b_1p^2-b_1q^2 & -2b_1pq & b_2\left(p^2+q^2\right)-\rho_2\omega^2 & 0 & 0\\ 2b_1pq & b_1p^2-b_1q^2 & 0 & b_2\left(p^2+q^2\right)-\rho_2\omega^2 & 0\\ -a_3p & -a_3q & 0 & 0 & a_6 \end{bmatrix} \tag{15}$$

2.4. General Solutions

Based on the theory of ordinary differential equations, the solutions of Eq. (12) are

$$\tilde{\boldsymbol{\theta}}\left(z\right)=\exp\left[\left(z-z_{p-1}\right)\tilde{\boldsymbol{A}}^{(p)}\left(\omega,k\right)\right]\tilde{\boldsymbol{\theta}}\left(z_{p-1}\right)\quad\left(z_{p-1}\le z\le z_p,\ p=1,2,\ldots,N\right) \tag{16}$$

where $\exp\left[\left(z-z_{p-1}\right)\tilde{\boldsymbol{A}}^{(p)}\left(\omega,k\right)\right]$ is the matrix exponential function.

Let $z = z_p$ in Eq. (16), and we find that

$$\tilde{\boldsymbol{\theta}}_1^{(p)} = \boldsymbol{T}^{(p)} \tilde{\boldsymbol{\theta}}_0^{(p)} \tag{17}$$

where $\tilde{\boldsymbol{\theta}}_1^{(p)}$ and $\tilde{\boldsymbol{\theta}}_0^{(p)}$ denote the state vectors on the upper and lower surfaces of the p-th layer, and $\boldsymbol{T}^{(p)} = \exp\left[(z_p - z_{p-1})\, \tilde{\boldsymbol{A}}^{(p)}(\omega, k)\right] = \exp\left[h_p \tilde{\boldsymbol{A}}^{(p)}(\omega, k)\right]$

Similarly, we get

$$\tilde{\boldsymbol{\theta}}_1^{(p+1)} = \boldsymbol{T}^{(p+1)} \tilde{\boldsymbol{\theta}}_0^{(p+1)} \tag{18}$$

2.5. Imperfect Bonding Conditions

According to the traditional analysis theory of composite layered structures, the connection conditions between interfaces are assumed to be perfect. Thus, stresses and displacements are continuous across interfaces. However, the interface slip and separation of the laminates may occur during service, which may lead to material failures. Therefore, it is necessary to study the imperfect interface of QC multilayered structures.

In this paper, the general spring model is employed to simulate the continuous and discontinuous interface conditions [31, 34] when the phason and phonon displacements and stresses are through the interfaces. The interface conditions of z_p for the weak connection between the p-th layer and the $(p+1)$-th layer are as follows

$$\begin{aligned}
\tilde{\sigma}_{xz}^{(p+1)} &= \tilde{\sigma}_{xz}^{(p)} = \beta_1^{(p)}\left(\tilde{u}_x^{(p+1)} - \tilde{u}_x^{(p)}\right)\\
\tilde{\sigma}_{yz}^{(p+1)} &= \tilde{\sigma}_{yz}^{(p)} = \beta_2^{(p)}\left(\tilde{u}_y^{(p+1)} - \tilde{u}_y^{(p)}\right)\\
\tilde{\sigma}_{zz}^{(p+1)} &= \tilde{\sigma}_{zz}^{(p)} = \beta_3^{(p)}\left(\tilde{u}_z^{(p+1)} - \tilde{u}_z^{(p)}\right)\\
\tilde{H}_{xz}^{(p+1)} &= \tilde{H}_{xz}^{(p)} = \gamma_1^{(p)}\left(\tilde{w}_x^{(p+1)} - \tilde{w}_x^{(p)}\right)\\
\tilde{H}_{yz}^{(p+1)} &= \tilde{H}_{yz}^{(p)} = \gamma_2^{(p)}\left(\tilde{w}_y^{(p+1)} - \tilde{w}_y^{(p)}\right)
\end{aligned} \tag{19}$$

where $\beta_i^{(p)}$ and $\gamma_k^{(p)}$ are the interface coefficients of the phonon and the phason fields, respectively. The case where $\beta_i^{(p)}$ and $\gamma_k^{(p)} \to \infty$ describes the perfect interface, whereas $\beta_i^{(p)}$ and $\gamma_k^{(p)} \to 0$ indicates that the p-th layer and the $(p+1)$-th layer are completely detached.

Eqs. (11) and (19) can be expressed as

$$\tilde{\boldsymbol{\theta}}_0^{(p+1)} = \boldsymbol{P}^{(p)} \tilde{\boldsymbol{\theta}}_1^{(p)} \tag{20}$$

where

$$\boldsymbol{P}^{(p)} = \begin{bmatrix} \boldsymbol{I} & \boldsymbol{P}_e^{(p)} \\ \boldsymbol{0} & \boldsymbol{I} \end{bmatrix} \tag{21}$$

with $\boldsymbol{I}$ an identity matrix and

$$\boldsymbol{P}_e^{(p)} = \begin{bmatrix} 1/\beta_1^{(p)} & 0 & 0 & 0 & 0 \\ 0 & 1/\beta_2^{(p)} & 0 & 0 & 0 \\ 0 & 0 & 1/\beta_3^{(p)} & 0 & 0 \\ 0 & 0 & 0 & 1/\gamma_1^{(p)} & 0 \\ 0 & 0 & 0 & 0 & 1/\gamma_2^{(p)} \end{bmatrix} \tag{22}$$

The relation of state vectors between the upper surface of the $(p+1)$-th layer and the lower surface of the p-th layer can be determined by solving Eqs. (17), (18), and (20):

$$\tilde{\boldsymbol{\theta}}_1^{(p+1)} = \boldsymbol{T}^{(p+1)} \boldsymbol{P}^{(p)} \boldsymbol{T}^{(p)} \tilde{\boldsymbol{\theta}}_0^{(p)} \tag{23}$$

Continuing the preceding procedure, we can further derive the solutions for the corresponding multilayered structure as

$$\tilde{\boldsymbol{\theta}}_1^{(N)} = \prod_{p=N}^{2} (\boldsymbol{P}^{(p)} \boldsymbol{T}^{(p-1)}) \boldsymbol{T}^{(1)} \tilde{\boldsymbol{\theta}}_0^{(1)} = \boldsymbol{M} \tilde{\boldsymbol{\theta}}_0^{(1)} \tag{24}$$

where the matrix $\boldsymbol{M}$ is the global propagator matrix.

We rewrite Eq. (24) as

$$\tilde{\boldsymbol{\theta}}_1^{(N)} = \left\{ \begin{array}{c} \boldsymbol{U}(H) \\ \boldsymbol{Y}(H) \end{array} \right\} = \begin{bmatrix} \boldsymbol{M}_{11} & \boldsymbol{M}_{12} \\ \boldsymbol{M}_{21} & \boldsymbol{M}_{22} \end{bmatrix} \tilde{\boldsymbol{\theta}}_0^{(1)} = \begin{bmatrix} \boldsymbol{M}_{11} & \boldsymbol{M}_{12} \\ \boldsymbol{M}_{21} & \boldsymbol{M}_{22} \end{bmatrix} \left\{ \begin{array}{c} \boldsymbol{U}(0) \\ \boldsymbol{Y}(0) \end{array} \right\} \tag{25}$$

where $\boldsymbol{U}(z) = \{\tilde{u}_x, \tilde{u}_y, \tilde{u}_z, \tilde{w}_x, \tilde{w}_y\}^{\mathrm{T}}$, $\boldsymbol{Y}(z) = \left\{\tilde{\sigma}_{xz}, \tilde{\sigma}_{yz}, \tilde{\sigma}_{zz}, \tilde{H}_{xz}, \tilde{H}_{yz}\right\}^{\mathrm{T}}$.

The traction on the bottom and top surfaces is assumed to be zero, so Eq. (25) can be rewritten as

$$\left\{ \begin{array}{c} \boldsymbol{U}(z_{N+1}) \\ \mathbf{0} \end{array} \right\} = \begin{bmatrix} \boldsymbol{M}_{11} & \boldsymbol{M}_{12} \\ \boldsymbol{M}_{21} & \boldsymbol{M}_{22} \end{bmatrix} \left\{ \begin{array}{c} \boldsymbol{U}(z_1) \\ \mathbf{0} \end{array} \right\} \tag{26}$$

where $\boldsymbol{M}_{11}$, $\boldsymbol{M}_{12}$, $\boldsymbol{M}_{21}$, and $\boldsymbol{M}_{22}$ are submatrices of the propagator matrix $\boldsymbol{M}$.

There are nonzero solutions in Eq. (26), and the submatrix $\boldsymbol{M}_{21}$ must satisfy

$$\det[\boldsymbol{M}_{21}] = 0 \tag{27}$$

Therefore, by solving Eq. (27), the dispersion relation of guided wave propagation can be obtained.

3. Numerical Studies

Illustrative examples of wave propagation in multilayered QC structures with imperfect interfaces are provided for dynamic analysis. It is assumed that the multilayered plate is composed of three single plates, and each layer has an equal thickness. The horizontal dimensions of the laminate are infinite, and its total thickness is H.

For ease of numerical calculation, the following dimensionless quantities will be used [39], which are

$$\begin{array}{l} C_{ef}^* = \frac{C_{ef}}{C_{\max}}\,(e,f=1,2,3,4),\ R_1^* = \frac{R_1}{R_{\max}},\ K_l^* = \frac{K_l C_{\max}}{R_{\max}^2}\,(l=1,2,4) \\ \rho_1^* = \frac{\rho_1}{\rho_{\max}},\ \rho_2^* = \frac{\rho_2 C_{\max}^3}{\rho_{\max} R_{\max}^3},\ \beta_i^* = \frac{1}{\beta_i C_{\max}},\ \gamma_k^* = \frac{R_{\max}^2}{\gamma_k C_{\max}} \end{array} \tag{28}$$

where $C_{\max}$, $R_{\max}$, and $\rho_{\max}$ are the maximum phonon elastic coefficient, phonon-phason coupling elastic coefficient, and mass density of the material, respectively.

Two kinds of materials are considered [2]: one is QC material Al-Ni-Co (called QC), and the other is crystal material $BaTiO_3$ (called C). And we have proved that the two materials' constants are completely in accord with the elastic deformation energy density [10, 40], so they can be used for calculating the dispersion characteristics of guided waves. In order to avoid the appearance of a singular matrix during calculation due to the lack of a phason field for $BaTiO_3$, we assume that the phason elastic constant K_l of the crystal is 10^{-8} times that of the QC [14].

3.1. Dispersion Relation

Figure 1 shows the dispersion curves of the first seven modes for the wave propagating in QC/QC/QC and C/C/C plates with perfect interfaces. The interface of the laminates is assumed to be perfectly bonded, and the orientation angle of wave propagation is 45°. The dispersion curves of the QC/QC/QC plate (Fig. 1a) are very similar to those of the C/C/C plate (Fig. 1b). Considering that the wave propagates to the bottom and top surfaces of the laminate, the transverse wave (S-wave) and the longitudinal wave (P-wave) will be converted, which can be superimposed in the plate to form a guided wave mode after a period of time, as shown in Fig. 1. Mode 1 is the lowest order dispersion curve of the transverse wave, and the change rate of the dimensionless phase velocity $c(c=\omega/\left(k\sqrt{C_{\max}/\rho_{\max}}\right))$ decreases as the dimensionless wavenumber kH increases and then tends to be stable in Fig. 1a, b. Mode 2 denotes the lowest mode of P-wave whose c is approximately constant as kH increases. The c of mode 3 starts to decrease from a specific value, and different stacking orders of the plates have different effects on this specific value. The dimensionless phase velocities c of mode 4, mode 5, mode 6, and mode 7 change obviously and gradually level off to mode 2, and they tend to infinity at $kH \to 0$.

To analyze the dispersion characteristics in more detail, dimensionless natural frequencies Ω ($\Omega = \omega H/\sqrt{C_{\max}/\rho_{\max}}$) of the six laminated plates at the dimensionless wave number $kH = 1$ are given in Table 1. These frequencies of six stacking sequence plates are relatively close to mode 1. Furthermore,

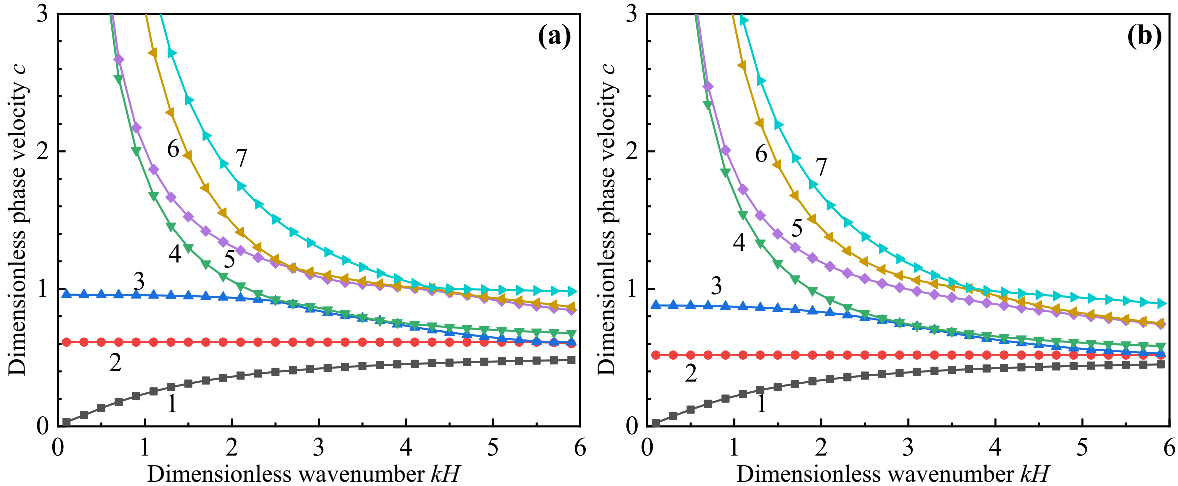

Fig. 1. Dispersion curves for QC/QC/QC plate (**a**) and C/C/C plate (**b**)

Table 1. **Dimensionless natural frequencies Ω at $kH = 1$**

Stacking sequences	Mode				
	1	2	3	4	5
QC/QC/QC	0.23696	0.61218	0.95328	1.82549	2.00308
QC/C/QC	0.25235	0.61865	0.97165	1.82566	2.03354
QC/QC/C	0.23503	0.61435	0.96806	1.84190	2.02330
C/C/QC	0.21437	0.52120	0.83713	1.60132	1.77906
C/QC/C	0.20060	0.52514	0.85275	1.60536	1.74687
C/C/C	0.21873	0.51776	0.87041	1.68067	1.84958

it can be observed that Ω of the QC/C/QC plate is the largest, which indicates that the rigidity of this laminate is highest. The dimensionless natural frequencies Ω of three-layer boards with different stacking orders can be roughly divided into two groups in Table 1: Group 1 is QC/QC/QC, QC/QC/C, and QC/C/QC; Group 2 covers C/C/QC, C/QC/C, and C/C/C. The difference of frequencies in different stacking sequences may be caused by the maximum phonon elastic modulus being higher than those of the crystal and the mass densities of the two materials being different. Therefore, by exciting the appropriate frequencies for different laminates, the material layups can be identified in the nondestructive evaluation technology.

3.2. Influence of Interfacial Imperfection on a QC Plate

In this part, the variation of the dispersion curves and mode shapes in a QC/QC/C plate with weak interfaces are presented. The dimensionless interface coefficient β_3^* is assumed to be zero [31, 34], and the other dimensionless interface coefficients are $\beta_1^* = \beta_2^* = \gamma_1^* = \gamma_2^* = \delta$. One identical set of the dimensionless interface coefficients δ in all interfaces are used for every laminate, and four kinds of δ are considered: δ =0, 0.3, 0.6, 0.9.

The dependence of the distribution of different modes (1, 2, 3, and 4) for the QC/QC/C plate on different interface coefficients is presented in Fig. 2. With the increase of δ, c (Fig. 2a–d) decreases for the same wavenumber kH. The dispersion curves in Fig. 2a, b are the lowest modes of the transverse wave and longitudinal wave, respectively. It is noticed that mode 1 is more sensitive to interface coefficients than mode 3 (Fig. 2c). According to crystal elasticdynamics, mode 2 in Fig. 1b is called the 0-order mode, and its phase velocity c is constant. However, comparing Figs. 2b and 1a with 1b, c of mode 2 is not a specific constant if there is QC material in the laminate. This feature indicates that mode 2 is affected by the QC phason field. In addition, the slopes of mode 4 (Fig. 2d) in the defective plate decrease with the increase of wavenumber.

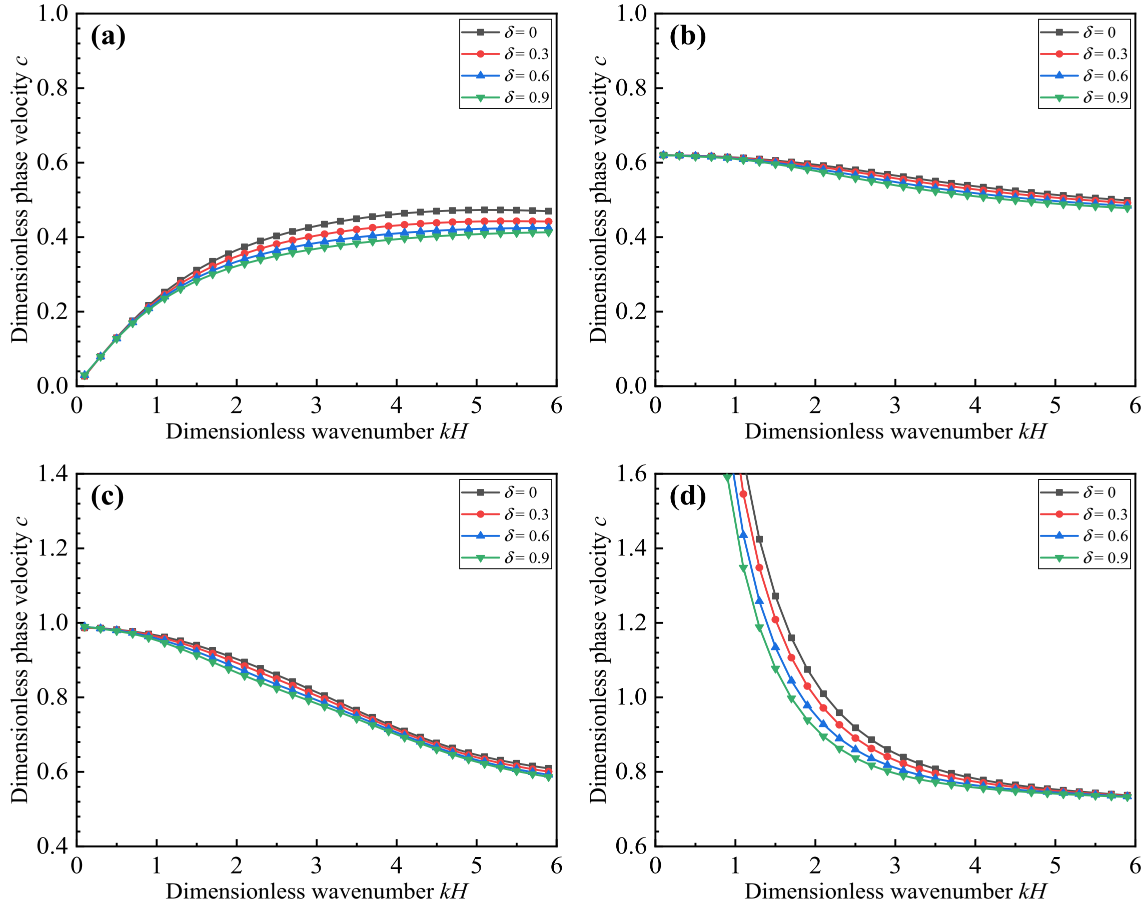

Fig. 2. Dispersion curves for QC/QC/C plate with different interface coefficients δ: **a** mode 1; **b** mode 2; **c** mode 3; **d** mode 4

The variations of the first-order and third-order mode shapes for the QC/QC/C plates with $kH = 2$ and $\alpha = 45°$ along the thickness direction are presented in Fig. 3. The distribution of the phonon dimensionless mode shapes u_x (Fig. 3a, d) for the laminate along the z-direction has the same value as u_y. Moreover, the variation of the third-order u_x is more sensitive to that of the first-order u_x. Despite the interface coefficient β_3 defined as zero, the phonon displacement mode shapes u_z (Fig. 3b, e) increase as the interface coefficient is larger. This feature indicates that the overall bending stiffness of the laminate continuously decreases due to the gradual weakening of the bonding surface. While the value of the phason dimensionless mode shapes w_x (Fig. 3c, f) is opposite to that of w_y. In addition, the discontinuity of the first-order w_x between layers becomes more weakened with the increases of interface coefficients, but the third-order w_x gets stronger at $z/H = 1/3$ and $z/H = 2/3$. w_x vary linearly in the QC layer and return to zero in the crystal layers. This transformation can be used to identify the stacking sequence of materials in the nondestructive evaluation technology. In addition, the distributions of displacement mode shapes of the next layer can also be predicted by selecting appropriate interface coefficients.

4. Conclusions

In this paper, the guided wave propagation in multilayered 2D QC plates with imperfect interfaces has been derived. The exact solution is achieved on the basis of the state vector approach and the propagator matrix method. Two kinds of laminates are used to investigate the dispersion curves with perfect interfaces, and the QC/QC/C plate is selected to analyze the influences of interface coefficients on the dispersion relation and displacement mode shapes. Some significant features are listed below:

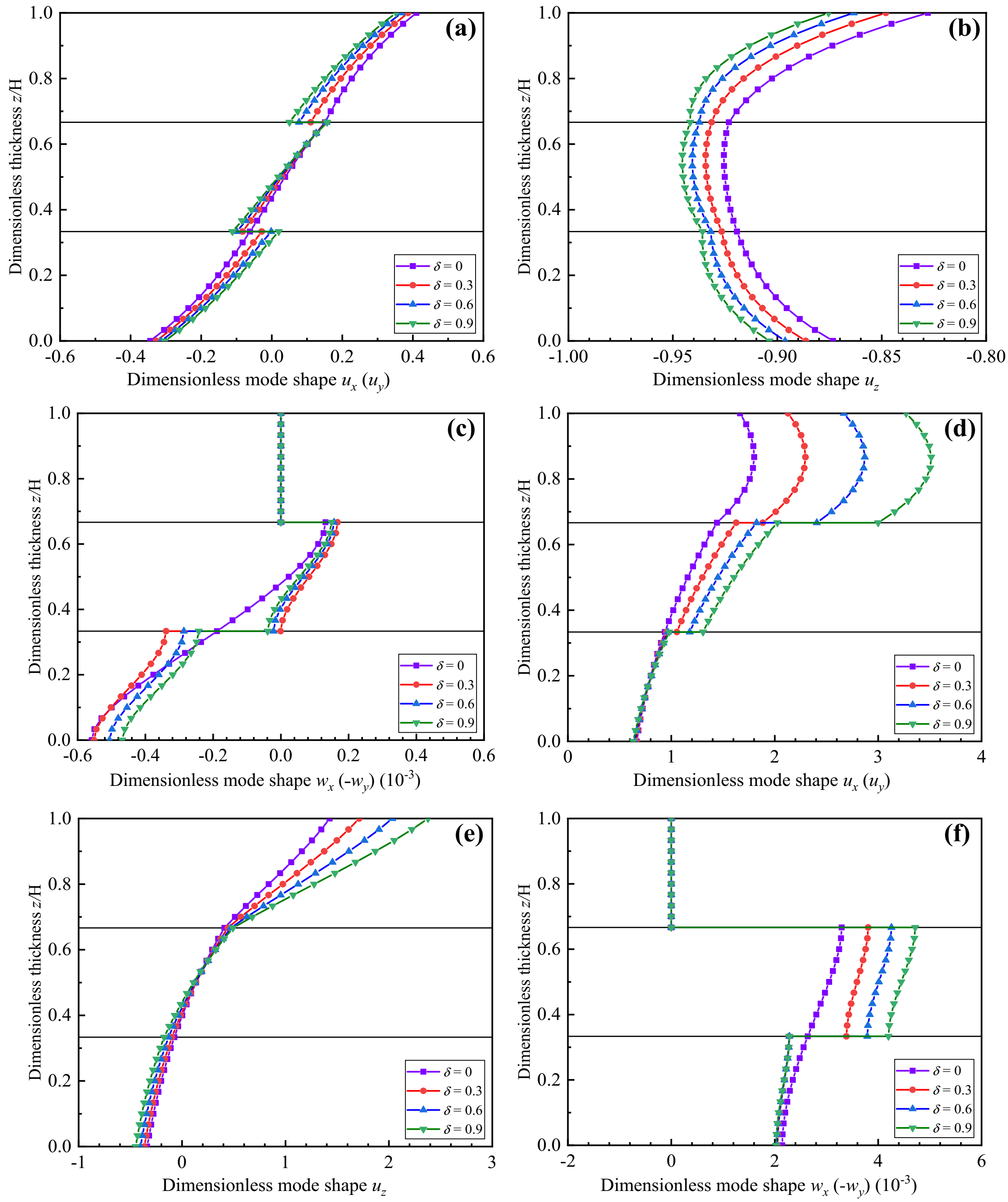

Fig. 3. The first-order mode shapes u_x (**a**), u_z (**b**), and w_x (**c**); the third-order mode shapes u_x (**d**), u_z (**e**), and w_x (**f**)

1. The state equations constructed in this paper are very effective and universal for deriving the general solutions of the state variables. Some special cases such as homogenous/inhomogenous QC plates and multi-physics coupling QC laminates could all be investigated from the present solutions.
2. Mode 2 denotes the lowest mode of P-wave. Different from the crystal plate, the phonon-phason coupling effect makes the phase velocity c of mode 2 in the QC plates decrease with the interface coefficients increasing.

3. The general dispersion curves depend on the interface coefficients. The weak interfaces reduce the natural frequency of the first four modes of the QC laminates, and different stacking orders also have an effect on the natural frequency. Therefore, the appropriate weak interface and the suitable stacking mode can be selected to optimize the dynamic characteristics of the QC plates.
4. The phason displacement mode shape w_x in different QC laminates could be utilized to identify the stacking sequence of materials. The distributions of displacement mode shapes can also be predicted by selecting the appropriate interface coefficients δ.

Finally, the results of the current study can be used to validate the accuracy of other numerical methods and serve the analysis and design of intelligent QC material laminates.

Acknowledgements. This work was supported by the National Natural Science Foundation of China (Grant Nos. 11972365, 12102458, and 11972354) and China Agricultural University Education Foundation (No. 1101-2412001).

Declarations

Conflict of interest No support, financial or otherwise, has been received from any organization that may have an interest in the submitted work; and there are no other relationships or activities that could appear to have influenced the submitted work.

References

[1] Levine D, Steinhardt PJ. Quasicrystals: a new class of ordered structures. Phys Rev Lett. 1984;53(26):2477–80.
[2] Fan TY. Mathematical theory of elasticity of quasicrystals and its applications. Heidelberg: Springer; 2011.
[3] Sakly A, Kenzari S, Bonina D, et al. A novel quasicrystal-resin composite for stereolithography. Mater Des. 2014;56(4):280–5.
[4] Cao ZJ, Ouyang LZ, Wang H, et al. Composition design of Ti–Cr–Mn–Fe alloys for hybrid high-pressure metal hydride tanks. J Alloy Compd. 2015;639:452–7.
[5] Bohra M, Pavan TM, Fournee V, et al. Growth, structure and thermal stability of quasicrystalline Al–Pd–Mn–Ga thin films. Appl Surf Sci. 2020;505:144494.
[6] Zhao MH, Fan CY, Lu CS, et al. Analysis of interface cracks in one-dimensional hexagonal quasi-crystal coating under in-plane loads. Eng Fract Mech. 2021;243(12):107534.
[7] Wang J, Lu C, Wang Q, et al. Influence of microstructures on mechanical behaviours of SiC nanowires: a molecular dynamics study. Nanotechnology. 2012;23(2):025703.
[8] Jaric MV, Nelson DR. Introduction to quasicrystals. Phys Today. 1990;43(3):77–9.
[9] Guo JH, Zhang M, Chen WQ, et al. Free and forced vibration of layered one-dimensional quasicrystal nanoplates with modified couple-stress effect. Sci China (Physics, Mechanics and Astronomy). 2020;63(07):124–5.
[10] Hu CZ, Wang RH, Ding DH. Symmetry groups, physical property tensors, elasticity and dislocations in quasicrystals. Rep Prog Phys. 2000;63(1):1–39.
[11] Li LH, Yun GH. Elastic fields around a nanosized elliptic hole in decagonal quasicrystals. Chin Phys B. 2014;23(10):106104.
[12] Yang LZ, Gao Y, Pan E, et al. An exact solution for a multilayered two-dimensional decagonal quasicrystal plate. Int J Solids Struct. 2014;51(9):1737–49.
[13] Guo JH, Yu J, Xing YM, et al. Thermoelastic analysis of a two-dimensional decagonal quasicrystal with a conductive elliptic hole. Acta Mech. 2016;227(9):2595–607.
[14] Li Y, Yang LZ, Zhang LL, et al. Nonlocal free and forced vibration of multilayered two-dimensional quasicrystal nanoplates. Mech Adv Mater Struct. 2021;28(12):1216–26.
[15] Huang YZ, Li Y, Zhang LL, et al. Dynamic analysis of a multilayered piezoelectric two-dimensional quasicrystal cylindrical shell filled with compressible fluid using the state-space approach. Acta Mech. 2020;231(6):2351–68.
[16] Li XF. Elastohydrodynamic problems in quasicrystal elasticity theory and wave propagation. Phil Mag. 2013;93(13):1500–19.
[17] Zhang B, Yu JG, Zhang XM, et al. Guided wave characteristics in the functionally graded two-dimensional hexagonal quasi-crystal plate. ZAMM-J Appl Math Mech/Z für Angew Math und Mech. 2020;100(11):201900210.
[18] Chen JY, Pan E, Chen HL. Wave propagation in magneto-electro-elastic multilayered plates. Int J Solids Struct. 2007;44(3–4):1073–85.

[19] Maghsoodi A, Ohadi A, Sadighi M. Calculation of wave dispersion curves in multilayered composite-metal plates. Shock Vib. 2014;2014:1–7.
[20] Wu B, Yu JG, He CF. Wave propagation in non-homogeneous magneto-electro-elastic plates. J Sound Vib. 2008;317(1–2):250–64.
[21] Benveniste Y. The effective mechanical behaviour of composite materials with imperfect contact between the constituents. Mech Mater. 1985;4(2):197–208.
[22] Li P, Jin F. Effect of an imperfect interface in a quartz crystal microbalance for detecting the properties of an additional porous layer. J Appl Phys. 2014;115(5):054502.
[23] Gupta S, Kundu S, Vishwakarma SK. Propagation of torsional surface waves in an inhomogeneous layer over an initially stressed inhomogeneous half-space. J Vib Control. 2015;21(7):1286–98.
[24] Chen TY, Hsieh CH, Chuang PC. A spherical inclusion with inhomogeneous interface in conduction. J Mech. 2003;19(1):1–8.
[25] Ru CQ, Schiavone P. A circular inclusion with circumferentially inhomogeneous interface in antiplane shear. Proc R Soc Lond. Ser A: Math Phys Eng Sci. 1997;453(1967): 2551–72.
[26] Hosten B, Castaings M. Finite elements methods for modeling the guided waves propagation in structures with weak interfaces. J Acoust Soc Am. 2005;117(3):1108–13.
[27] Diaz AD, Chataigner S, Caron JF. A layerwise finite element for multilayers with imperfect interfaces. Compos Struct. 2011;93(12):3262–71.
[28] Alaimo A, Milazzo A, Orlando C. Boundary elements analysis of adhesively bonded piezoelectric active repair. Eng Fract Mech. 2009;76(4):500–11.
[29] Gu CL, Li P, Jin F, et al. Effects of the imperfect interface and viscoelastic loading on vibration characteristics of a quartz crystal microbalance. Acta Mech. 2018;229(7):2967–77.
[30] Wang GL, Liu JX, Feng WJ, et al. Mechanically, electrically and magnetically imperfect interface conditions via first-order plate theory. Mech Res Commun. 2018;94:110–3.
[31] Wang X, Pan E. Exact solutions for simply supported and multilayered piezothermoelastic plates with imperfect interfaces. Open Mech J. 2007;1(1):1–10.
[32] Vattré A, Pan E. Thermoelasticity of multilayered plates with imperfect interfaces. Int J Eng Sci. 2021;158:103409.
[33] Vattré A, Pan E, Chiaruttini V. Free vibration of fully coupled thermoelastic multilayered composites with imperfect interfaces. Compos Struct. 2021;259:113203.
[34] Chen WQ, Cai JB, Ye GR. Exact solutions of cross-ply laminates with bonding imperfections. AIAA J. 2003;41(11):2244–50.
[35] Zhao MH, Fan CY, Lu CS, et al. Interfacial fracture analysis for a two-dimensional decagonal quasi-crystal coating layer structure. Appl Math Mech. 2021;42(11):1633–48.
[36] Wang HT, Guo JH. Bending deformation of one-dimensional hexagonal piezoelectric quasicrystal layered plates with imperfect interface. In 2020 15th symposium on piezoelectrcity. Acoustic waves and device applications (SPAWDA). 2021:268–72.
[37] Bak P. Symmetry, stability, and elastic properties of icosahedral incommensurate crystals. Phys Rev B. 1985;32(9):5764–72.
[38] Bak P. Phenomenological theory of icosahedral incommensurate (quasiperiodic) order in Mn–Al alloys. Phys Rev Lett. 1985;54(14):1517–9.
[39] Wu D, Zhang LL, Xu WS, et al. Electroelastic Green's function of one-dimensional piezoelectric quasicrystals subjected to multi-physics loads. J Intell Mater Syst Struct. 2017;28(12):1651–61.
[40] Hu CZ, Wang RH, Ding DH, et al. Piezoelectric effects in quasicrystals. Phys Rev B. 1997;56(5):2463–8.